Intelligence modeling in electromechanical systems

www.imes.reapress.com

Intell. Model. Electromech. Syst. Vol. 2, No. 1 (2025) 48–64.

Paper Type: Original Article

Techno-Economic Modeling and Optimization of a Hybrid Wind–Solar Off-Grid System for Remote Areas

Sheis Khosravi*

Department of Electrical Engineering, Ayandegan University, Mazandaran, Tonekabon, Iran; Sheys.khosravi@gmail.com.

Citation:

Received: 04 September 2024 *Revised: 25 October 2024* *Accepted: 14 December 2024*	Khosrsvi, Kh. (2025). Techno-economic modeling and optimization of a hybrid wind–solar off-grid system for remote areas. *Intelligence modeling in electromechanical systems, 2*(1), 48-64.

Abstract

The primary objective of this study is to examine the optimal integration of wind and solar renewable energy resources within distribution networks. With the increasing penetration of wind farms into modern power systems, it has become evident that, similar to solar power plants, wind power facilities are subject to inherent uncertainties in electricity generation due to the stochastic nature of wind. Consequently, despite the low cost associated with wind-based electricity production, their large-scale deployment remains limited, as network operators continue to depend on thermal power plants to reliably satisfy load demands. A promising strategy to mitigate the uncertainty associated with renewable generation is the combined utilization of wind and solar power, wherein wind generation can supply the load during periods of low solar irradiation, while solar output can offset reduced wind generation during midday hours.

Keywords: Renewable energy, Wind energy, Solar energy, Distribution network, Optimization

1 | Introduction

With the growing global concerns regarding environmental pollution and the pressing need for sustainable energy solutions, renewable energy sources have gained considerable attention in modern microgrids [1]. Wind and solar energy, in particular, are abundant, cost-effective, and environmentally friendly, making them highly attractive for both on-grid and off-grid power generation systems. However, their intermittent nature introduces significant challenges in maintaining a reliable and stable power supply, which necessitates the adoption of advanced control strategies and comprehensive energy management techniques [2].

Hybrid Renewable Energy Systems (HRES), which integrate wind and solar power, have emerged as an effective solution to address the variability and intermittency of individual sources. By enabling complementary operation—where wind turbines supply energy during periods of low solar irradiance and Photovoltaic (PV) arrays compensate during times of weak wind conditions—hybrid systems enhance both

Corresponding Author: Sheys.khosravi@gmail.com

https://doi.org/10.48314/imes.vi.31

reliability and cost-effectiveness. In off-grid microgrids, such configurations typically employ a common Direct Current (DC) bus or a back-to-back Voltage Source Converter (VSC) to interface the renewable sources, while Battery Energy Storage Systems (BESS), connected via bidirectional DC-DC converters, provide load support and mitigate the adverse impacts of power generation fluctuations [3].

To maximize efficiency in HRES, accurate tracking of the Maximum Power Point (MPP) is essential. This study investigates advanced Maximum Power Point Tracking (MPPT) techniques for wind–solar hybrid systems operating under islanded conditions. Several MPPT algorithms are examined, including Perturb and Observe (P&O), Incremental Conductance, and neural network–based methods, which are further classified into model-dependent and model-independent approaches [4]. Model-dependent techniques utilize initial PV module parameters such as irradiance, temperature, open-circuit voltage, and short-circuit current to generate control signals, while model-independent approaches rely on real-time voltage and current measurements. Hybrid MPPT strategies integrate these methods with detailed solar panel modeling to enhance tracking accuracy, taking into account nonlinear effects such as series and parallel resistance, thermal voltage, and diode saturation current—all of which are strongly temperature-dependent and iteratively updated [5–7].

Moreover, the integration of high-penetration renewable energy sources into distribution networks introduces several critical technical challenges, including voltage fluctuations, reverse power flow, and potential overloading. Conventional voltage regulation methods, such as tap-changing transformers, prove inadequate under highly variable generation and load conditions, thereby emphasizing the need for more advanced control schemes and effective energy storage solutions [6]. To address these challenges, this study proposes an optimized control and simulation framework implemented in HOMER software to evaluate microgrid performance, taking into account environmental variability, load profiles, and the dynamic interactions among wind, solar, and storage components.

In summary, this research aims to develop a comprehensive and optimized control strategy for a wind–solar hybrid microgrid that maximizes power extraction, enhances system reliability, and mitigates technical challenges arising from the high penetration of renewable energy sources, thereby providing a technically robust and economically sustainable solution for remote and off-grid power supply [7–10].

2 | Methodology

In this study, a comprehensive modeling and simulation framework for HRES, integrating wind and PV power plants, is proposed. The methodology encompasses three main aspects: system modeling, energy conversion and control, and MPPT strategies [11].

2.1 | System Modeling

The wind energy subsystem is modeled using aerodynamic and electromechanical equations, with wind speed variations—including turbulence effects modeled via the Kaimal spectrum—explicitly incorporated. The Doubly-Fed Induction Generator (DFIG) is simulated by representing both rotor and stator dynamics, and a PWM-based converter is employed to regulate both active and reactive power. The PV subsystem is modeled using the standard equivalent circuit approach, capturing the I–V and P–V characteristics of solar cells under varying irradiance and temperature conditions. The hybrid system configuration also integrates energy storage and auxiliary backup generation units to ensure overall system reliability and stability [12].

2.2 | Energy Conversion and Control

Both subsystems are interfaced via power electronic converters. For the wind system, vector control techniques are applied to the DFIG to achieve decoupled control of torque and reactive power. The PV system is connected to the grid through a DC–DC converter, providing both voltage regulation and power optimization. At the system level, control strategies coordinate the interaction between renewable sources and the storage unit, maintaining power quality and minimizing power fluctuations under variable environmental conditions [13], [14].

2.3 | MPPT Techniques

To maximize energy extraction, MPPT algorithms are implemented for the PV array. Conventional Perturb-and-Observe (P&O) and incremental conductance methods are applied, alongside advanced intelligent approaches utilizing artificial neural networks. These algorithms dynamically adjust the operating point of the PV system to achieve optimal power generation under varying irradiance and temperature conditions. The control strategies are validated through comprehensive simulations, ensuring efficient, reliable, and stable operation of the hybrid system [14–16].

3 | Investigation of MPPT Methods for Solar Energy Systems

To investigate MPPT techniques for solar energy systems, the characteristics of solar energy in distributed generation were first analyzed. Solar energy is particularly well-suited for distributed power generation due to its wide availability, minimal environmental impact, and scalability [9]. These systems can be safely installed in residential and commercial environments without posing significant health risks. Estimates indicate that approximately 40% of generated energy is consumed within buildings, primarily for lighting, heating, and air conditioning. PV systems, in particular, can meet urban energy demands without necessitating extensive expansion of distribution networks. This study focuses on MPPT techniques to enhance the efficiency of solar cells, which generate DC subsequently converted to Alternating Current (AC) via power electronic converters [15].

A critical aspect of designing and operating solar energy systems is the development of efficient MPPT strategies. MPPT aims to optimize the power output of solar cells, which depends on environmental factors such as ambient temperature, solar irradiance, and load impedance [17]. Under constant temperature and irradiance conditions, each solar cell exhibits an optimal operating point at which power output is maximized. Identifying this point is essential for achieving economic efficiency and optimal system performance. In this study, various MPPT methods were evaluated, differing in algorithmic complexity, response speed, cost, and hardware requirements. These methods are broadly classified into two categories: online (model-independent) and offline (model-based). Offline methods rely on predefined solar cell models to calculate the optimal operating point, while online methods operate dynamically without requiring an explicit model [18–20].

4 | Case Study: Hybrid Wind–Solar Power Plant in Bandar Lengeh

4.1 | Regional Assessment

The proposed HRES is designed for a remote, mountainous region in Bandar Lengeh, southern Iran. Due to its unique geographical and climatic characteristics, the area experiences both significant solar irradiance and seasonal wind patterns, making it highly suitable for the integration of solar PV and wind energy resources. Prior to system design, a detailed assessment of the local climate was conducted, including the estimation of monthly average wind speeds and solar radiation levels. This climatic analysis forms the basis for selecting appropriate system components and ensures a reliable energy supply in an off-grid setting [21].

4.2 | System Components and Modeling

The hybrid configuration consists of three major subsystems:

I. Solar PV array: modeled using the single-diode equivalent circuit, capturing the I–V and P–V characteristics under varying irradiance and temperature. The array is interfaced with a DC–DC converter to regulate voltage and implement MPPT.

II. Wind turbine system: simulated using aerodynamic and electromechanical models, where wind speed inputs generate mechanical torque, subsequently converted into electrical power through a DFIG. A back-to-back PWM converter ensures independent control of active and reactive power.

III. Energy storage system: battery units are incorporated to balance supply and demand, enhance reliability, and mitigate the intermittency of renewable sources. The storage system is modeled with charging/discharging constraints and integrated via a bidirectional DC–DC converter.

IV. Converters and controllers: power electronic interfaces are modeled to coordinate the operation of PV, wind, and battery units, while implementing vector control strategies and MPPT algorithms to maximize system efficiency.

4.3 | Economic and Technical Analysis

The technical and economic feasibility of the hybrid system is evaluated using the HOMER software [18]. All relevant cost parameters, including Capital Expenditure (CAPEX), replacement costs, and Operation and Maintenance (O&M) expenses, are accurately entered for each component. The optimization module of HOMER is used to identify the most cost-effective configuration that satisfies the local load demand while ensuring high reliability. Key performance indicators such as Levelized Cost of Energy (LCOE), renewable fraction, and Net Present Cost (NPC) are calculated to compare alternative system configurations [19]. This integrated techno-economic analysis provides a reliable framework for decision-making in the deployment of hybrid renewable systems in remote and inaccessible regions.

5 | Hybrid System Configuration

A HRES typically consists of renewable energy sources operating in parallel with a non-renewable backup unit as well as an energy storage system. In this study, the proposed hybrid system comprises two primary renewable sources: wind and solar. The key components include a wind turbine, a PV array, a battery storage unit, and a power conversion device (inverter). *Fig. 1* presents the overall configuration of the hybrid system, modeled in HOMER software. Detailed specifications and modeling approaches for each component are discussed in the subsequent sections [21].

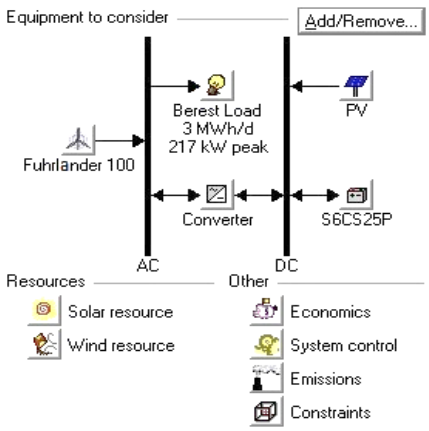

Fig. 1. The model of the standalone power generation system in HOMER software.

5.1 | Electrical Load

In this study, the load demand of a remote location is modeled as an off-grid (standalone) system [19]. The average daily electricity consumption at the site is estimated to be approximately 3 MWh/day, with a peak demand of around 217 kW. The daily load profile for a representative day is depicted in Figure 4-1. As shown, the maximum load reaches 160 kW at 23:00, while the minimum load of 96 kW occurs at 07:00. The HOMER software, accounting for climatic conditions and seasonal variations, generates the monthly load profiles, which are presented in *Fig. 2*.

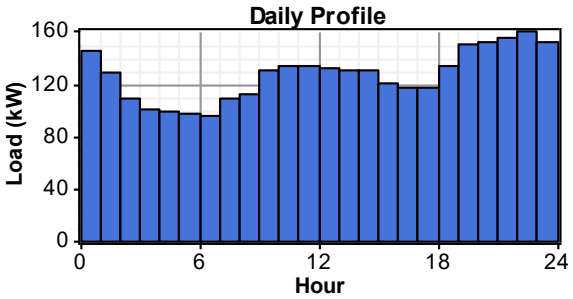

Fig. 2. Daily load profile.

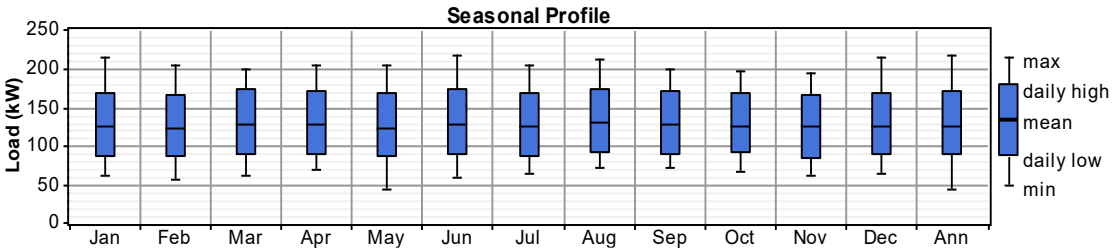

Fig. 3. Monthly electrical load profile of the region.

Figs. 4 and *5* are annual electrical load profile of the site over 8,760 hours, estimated by the software, with monthly breakdowns presented as a to *Fig. 5(l)*.

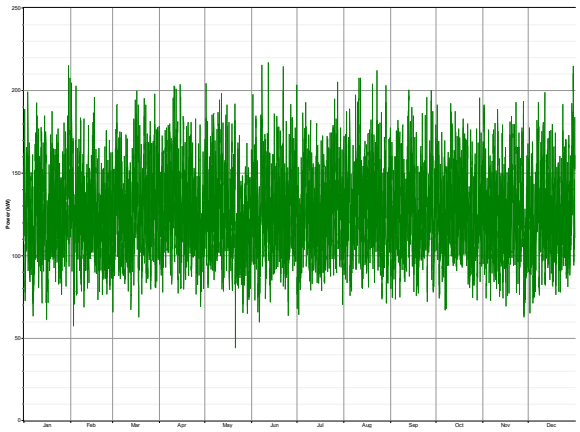

Fig. 4. Annual electrical load profile.

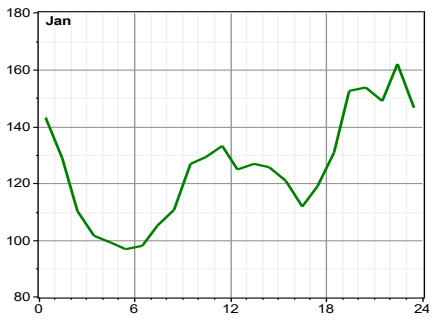

a.

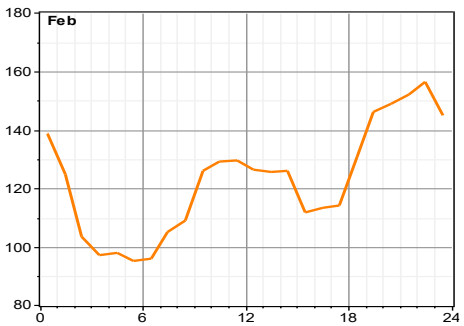

b.

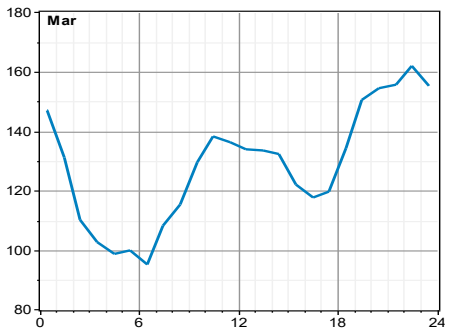

c.

d.

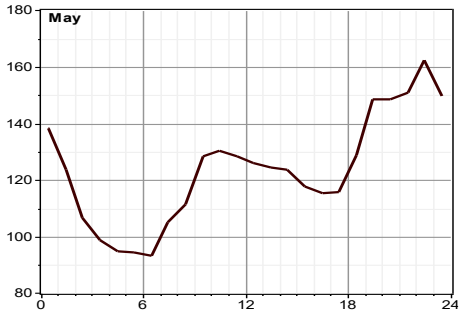

e.

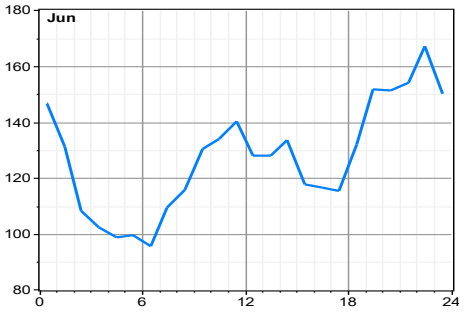

f.

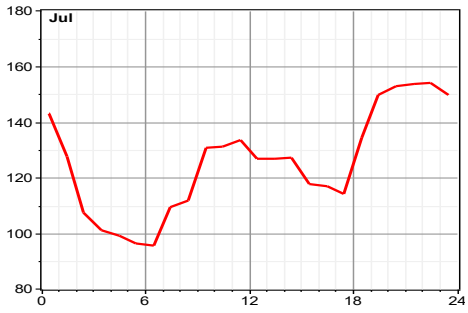

g.

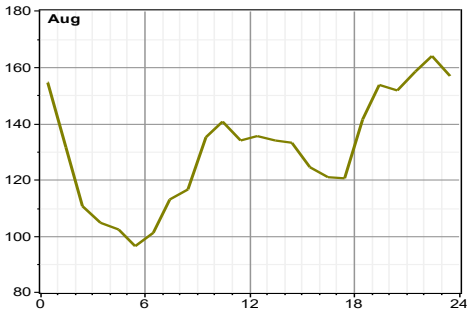

h.

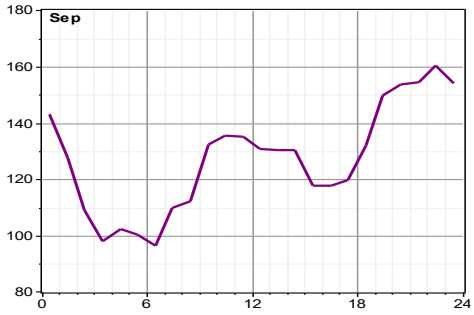

i.

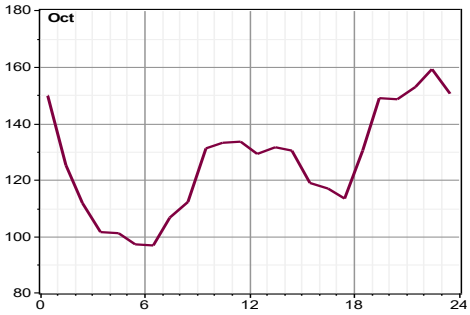

j.

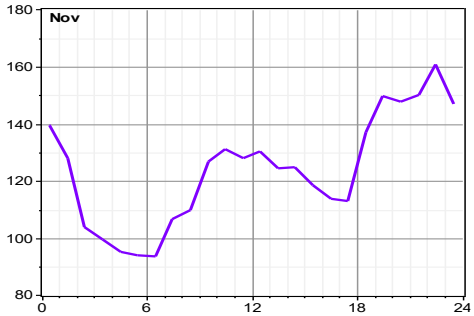

k.

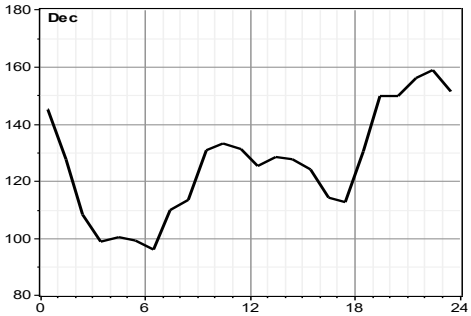

l.

Fig. 5. monthly electrical load profile.

5.2 | Wind and Solar Energy Resources

Wind and solar energy sources are utilized in this study. The required data were collected from the regional synoptic meteorological station. Monthly average wind speed and solar radiation data over a five-year period were employed for the analysis [20–22]. *Fig. 6* presents the monthly average wind speeds across the year, as modeled in HOMER software. By applying the monthly average wind speed, HOMER generates 8,760 hourly wind speed data points for a full year, as illustrated in *Fig. 7*. This annual wind profile is further detailed for each month in *Figs. 8 (a)* to *(l)*.

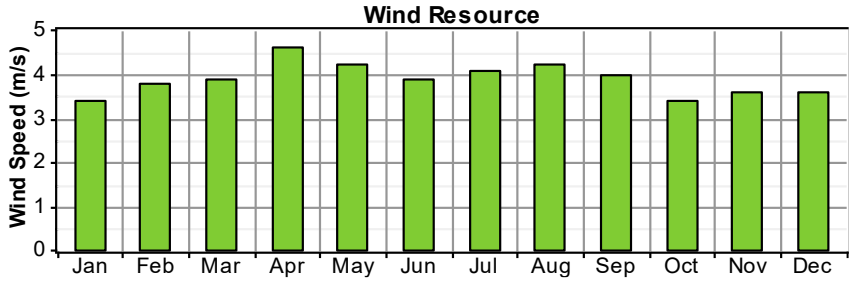

Fig. 6. Monthly average wind speed of the region.

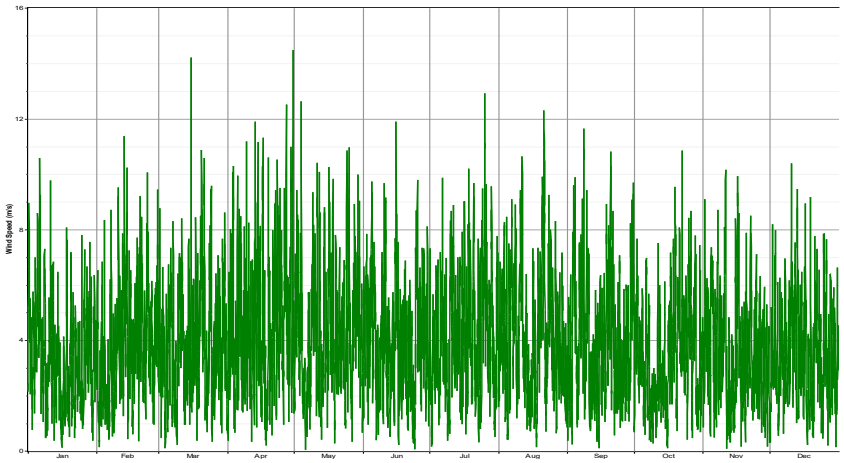

Fig. 7. Annual electrical load profile.

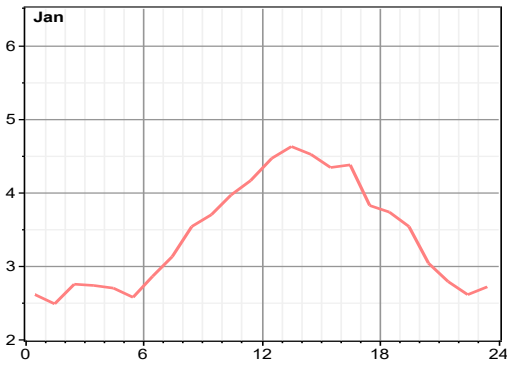

a.

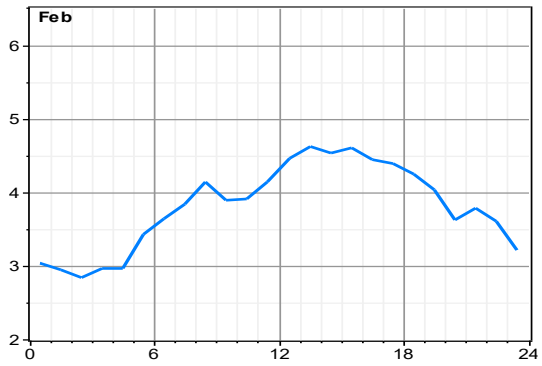

b.

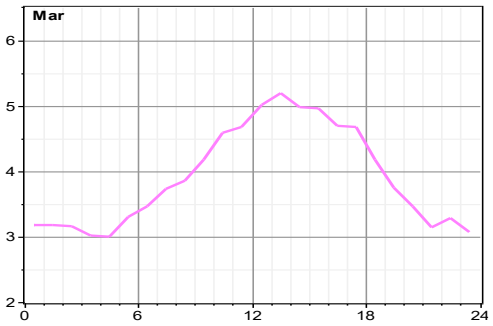
Mar
6
5
4
3
2
0
6
12
18
24

c.

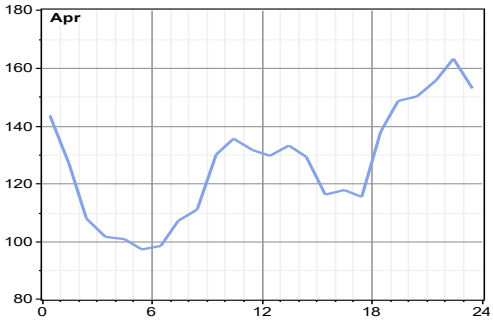
Apr
180
160
140
120
100
80
0
6
12
18
24

d.

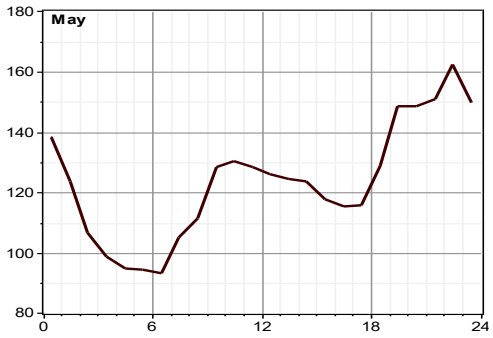
May
180
160
140
120
100
80
0
6
12
18
24

e.

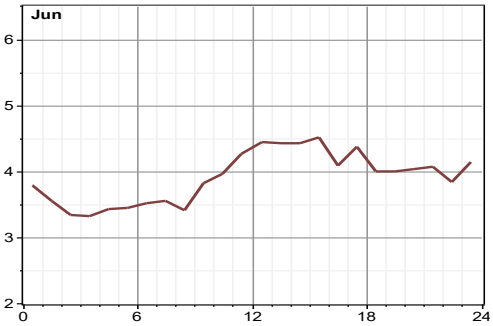
Jun
6
5
4
3
2
0
6
12
18
24

f.

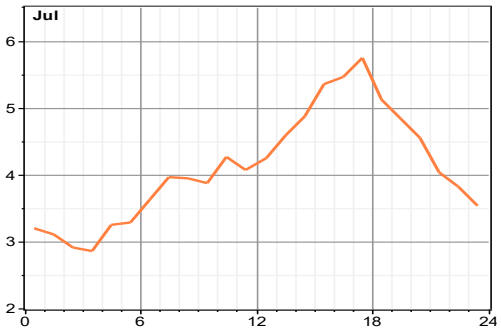
Jul
6
5
4
3
2
0
6
12
18
24

g.

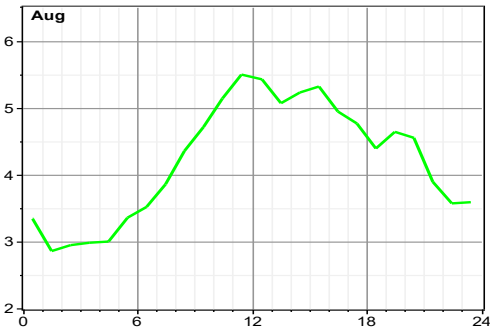
Aug
6
5
4
3
2
0
6
12
18
24

h.


Sep
6
5
4
3
2
0
6
12
18
24

i.

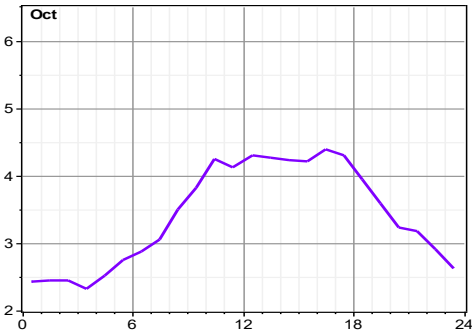
Oct
6
5
4
3
2
0
6
12
18
24

j.

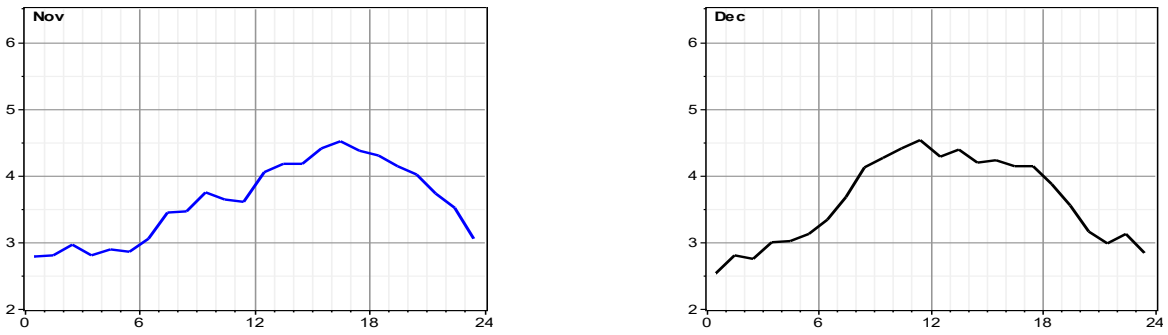

k. l.

Fig. 8. monthly wind speed data throughout the year.

Fig. 9 presents the Cumulative Distribution Function (CDF) of the region's wind speeds. In these calculations, the Weibull shape parameter (representing wind speed variability throughout the year) is 1.97, and the autocorrelation coefficient of wind speed is 0.85.

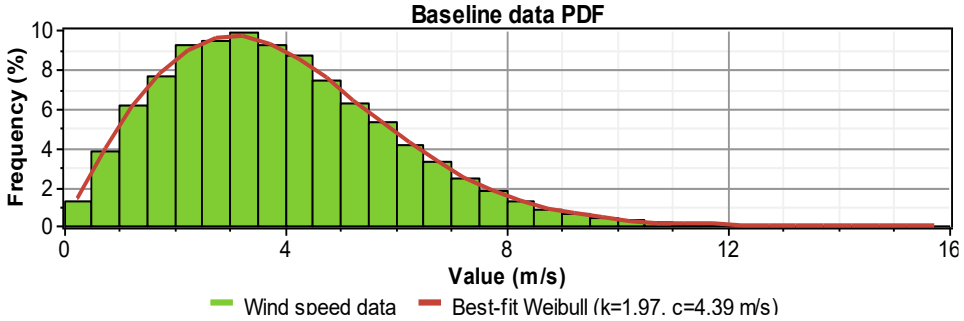

Fig. 9. CDF of the region's wind speed.

Fig. 10 presents the monthly average solar irradiation data as modeled in HOMER. The red line represents the clearness index, defined as the ratio of solar radiation at the Earth surface to the solar radiation at the top of the atmosphere, ranging from 0 to 1 to indicate atmospheric transparency.

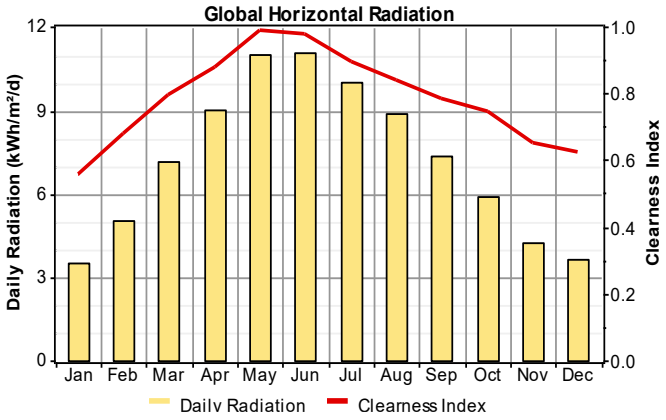

Fig. 10. Monthly average solar irradiation in HOMER.

In this study, the Fuhrländer wind turbine model is employed [20]. This turbine has a rated power of 100 kW and operates on AC. The capital cost per unit is estimated at 100,000 USD, while the replacement and Operation & Maintenance (O&M) costs are 80,000 USD and 50 USD, respectively. The turbine's power performance curve is depicted in *Fig. 11*, and its associated cost curves are shown in *Fig. 12*.

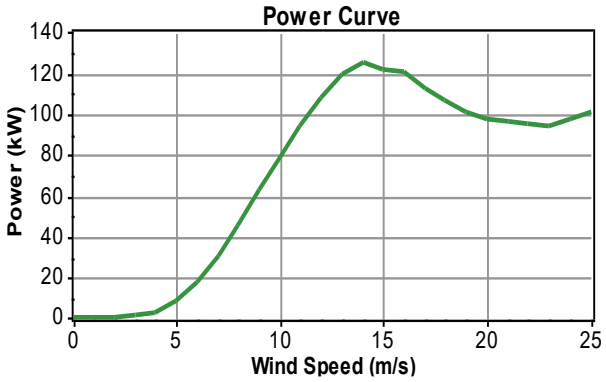

Fig. 11. Power output characteristic of the Fuhrländer wind turbine.

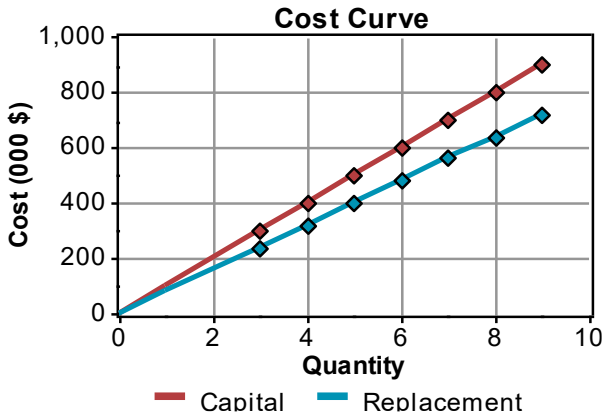

Fig. 12. Cost curve of the Fuhrländer wind turbine.

Since the wind speed data were sampled at height of 10 meters and the turbine hub height is 35 meters, HOMER employs *Eq. 1* to estimate the wind speed at the desired height.

$$V_w^h = V_w^{ref} \times \left(\frac{h}{h_{ref}}\right)^{\alpha}. \quad (1)$$

In this equation, v_w^h represents the wind speed at height h, while v_w^{ref} denotes the wind speed measured at the reference height h_{ref} in meters per second. The exponent α\alphaα is considered to be (1/7).

In this modeling, fixed (non-tracking) PV arrays are employed. The installation and replacement costs for a 1 kW system are considered to be 3,000 USD and 2,500 USD, respectively. The cost curve of the solar array is illustrated in *Fig. 13*.

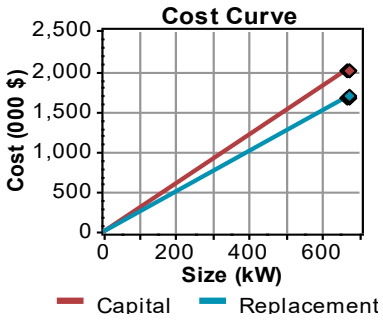

Fig. 13. Cost curve of the PV array.

For energy storage, the Surrette 6CS25P battery is employed, with specifications of 9.645 kWh, 1156 Ah, and 6 V, and can be modeled within HOMER. The installation, replacement, and O&M costs per battery unit are assumed to be $500, $450, and $6, respectively. The corresponding battery cost curve is depicted in *Fig. 14*.

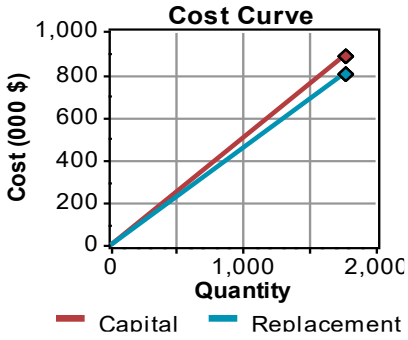

Fig. 14. Battery unit cost curve.

Since the system's consumers require AC, a power electronic inverter is necessary to interface DC generation sources with the AC load. For a 1 kW system, the installation, replacement, and maintenance costs of the inverter are assumed to be 800 USD, 750 USD, and 10 USD, respectively. The inverter cost curve is depicted in *Fig. 15*.

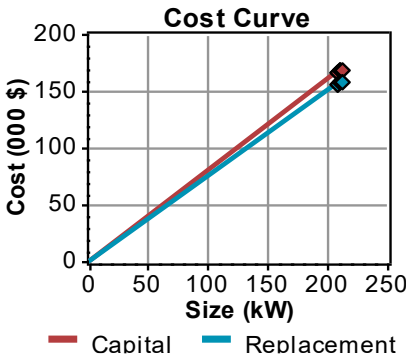

Fig. 15. Power inverter cost curve.

HOMER software utilizes the NPC methodology to evaluate the system's lifecycle cost [17–21]. The NPC is defined as the difference between the present value of all expenses incurred over the project duration and the present value of the revenues generated. All costs and revenues are evaluated using a fixed interest rate throughout the year. To account for the effect of inflation, the real interest rate, which considers both inflation and variations in the nominal interest rate, is applied in the NPC computation. The real interest rate, denoted as r, is calculated according to *Eq. 2*, where i represents the nominal interest rate and f represents the inflation rate.

$$i = \frac{i' - f}{i + f}. \tag{2}$$

The NPC is the primary output of the economic calculations in HOMER software and is computed using *Eq. 3*.

$$C_{NPC} = \frac{C_{ann,tot}}{CRF(i, R_{pro})}. \tag{3}$$

Here, $C_{ann,tot}$ represents the total annual cost, R_{Pro} is the project duration, and i is the real interest rate. The Capital Recovery Factor (CRF) over N years is defined by *Eq. 4*.

$$\mathrm{CRF(i,N)} = \frac{\mathrm{i(1+i)N}}{\mathrm{(1+i)N-1}}. \quad (4)$$

Another key parameter in the economic analysis of distributed generation units and in selecting the optimal system configuration, as calculated by HOMER, is the Cost of Energy (COE), defined as the average cost per kW of useful energy produced by the system. In the optimization process, the best configuration is selected from all possible arrangements [13]. The optimal configuration is defined as the one that satisfies all pre-defined constraints established by the operator while minimizing the NPC. In HOMER, all possible scenarios are simulated, ranked according to their NPC, and the feasible configuration with the lowest NPC is ultimately identified as the optimal configuration. Prior to performing simulations, a search space specifying the sizes of the components and the hybrid system must be defined in HOMER, enabling the software to evaluate different configurations. *Table 1* presents the HOMER search space for solar arrays, wind turbines, batteries, and power converters.

Table 1. HOMER search space for the components of the hybrid system.

	PV Array (kW)	FL100 (Quantity)	S6CS25P (Quantity)	Converter (kW)
1	668.000	3	1.773	208.00
2	669.000	4	1.774	209.00
3	670.000	5	1.775	210.00
4	671.000	6	1.776	211.00
5	672.000	7	1.777	212.00

The optimization results are presented in *Fig. 17*. As observed, the possible system configurations are sorted based on increasing Total NPC. For supplying electricity to a site with a maximum load demand of 217 kW and an energy consumption of 3 MWh/day, the optimal configuration consists of:

I. 669 kW of PV arrays.

II. 7 Fuhrlaender 100 kW wind turbines.

III. 1,775 units of Surrette 6CS25P batteries.

IV. 209 kW of power converters (inverters).

The NPC for this system is calculated as $4,825,298, and the COE is $0.342 per kWh. *Fig. 18* illustrates the percentage contribution of wind and solar energy in meeting the region's electricity demand.

PV (kW)	FL100	S6CS25P	Conv. (kW)	Initial Capital	Operating Cost ($/yr)	Total NPC	COE ($/kWh)	Ren. Frac.
669	7	1775	209	$ 3,761,700	83,202	$ 4,825,298	0.342	1.00
668	7	1775	212	$ 3,761,100	83,265	$ 4,825,502	0.342	1.00
669	7	1774	210	$ 3,762,000	83,207	$ 4,825,665	0.342	1.00
669	7	1777	208	$ 3,761,900	83,221	$ 4,825,746	0.342	1.00
670	7	1773	208	$ 3,762,900	83,149	$ 4,825,827	0.342	1.00
668	7	1777	211	$ 3,761,300	83,284	$ 4,825,951	0.342	1.00
669	7	1773	211	$ 3,762,300	83,212	$ 4,826,032	0.342	1.00
669	7	1776	209	$ 3,762,200	83,226	$ 4,826,113	0.342	1.00
668	7	1776	212	$ 3,761,600	83,289	$ 4,826,318	0.342	1.00
669	7	1775	210	$ 3,762,500	83,232	$ 4,826,480	0.342	1.00
670	7	1774	208	$ 3,763,400	83,174	$ 4,826,642	0.342	1.00

Fig. 16. illustrates the possible system configurations sorted according to increasing Total NPC.

Cost Summary | Cash Flow | Electrical | PV | FL100 | Battery | Converter | Emissions | Hourly Data

Production	kWh/yr	%
PV array	1,544,659	67
Wind turbines	764,915	33
Total	2,309,574	100

Consumption	kWh/yr	%
AC primary load	1,103,224	100
Total	1,103,224	100

Fig. 17. shows the contribution of wind and solar energy sources in meeting the load demand.

As shown in the figure, approximately 67% of the region's energy demand is supplied by the solar arrays, which is attributed to the favorable average solar irradiance of 6.93 kWh/m² in the area. In contrast, due to the relatively low average wind speed (3.89 m/s), only about 33% of the required energy is generated by the wind turbines. *Fig. 19* presents the monthly energy production of the hybrid system, highlighting the contributions of solar arrays and wind turbines in meeting the region's peak load. A summary of the cash flow for the proposed hybrid system is provided in *Fig. 20*, showing the NPC breakdown among solar arrays, wind turbines, batteries, and power converters.

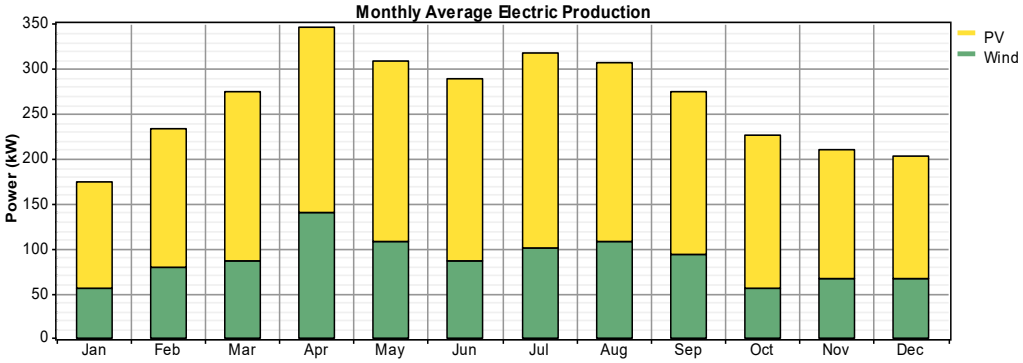

Fig. 18. Monthly energy production of the hybrid system, showing the contributions of wind turbines and solar arrays

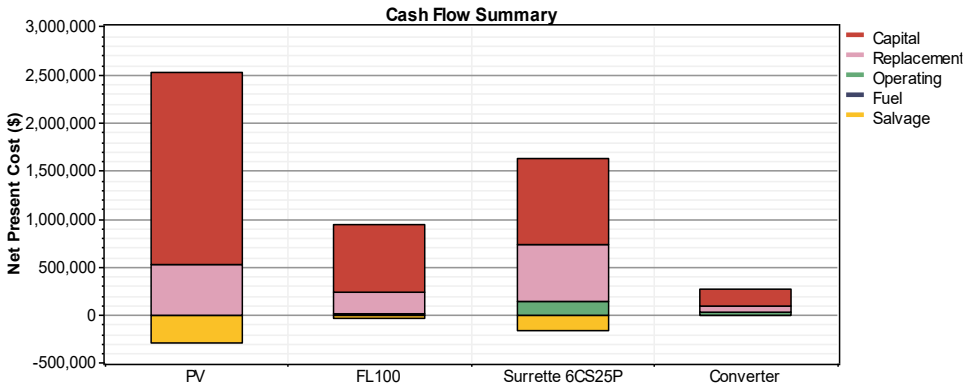

Fig. 19. Summary of the cash flow for the hybrid system.

6 | Sensitivity Analysis

Considering that the site is located in a mountainous region, higher wind speeds are expected. Therefore, in this study, average wind speeds of 3.89, 4, 5, 6, and 7 m/s and average solar irradiations of 5, 5.5, 6, and 6.93 kWh/m²/day are selected as sensitivity variables. After performing the simulations, HOMER identifies the optimal hybrid system configuration corresponding to an average wind speed of 7 m/s and an average solar irradiation of 6 kWh/m²/day, as shown in *Fig. 21*. The recommended configuration consists of 285 kW of PV arrays, six Fuhrländer 100 kW wind turbines, 1,350 units of S6CS25P batteries, and a 212-kW power converter. The NPC of this hybrid system is estimated at $3,070,934, and the COE for useful electricity

production is \$0.218/kWh. As illustrated in *Fig. 22*, with the increased average wind speed, 82% of the required energy is supplied by wind turbines, while the remaining 18% is provided by the PV arrays.

Sensitivity Results | Optimization Results

Sensitivity variables

Global Solar (kWh/m²/d) 6 Wind Speed (m/s) 7

Double click on a system below for simulation results.

PV (kW)	FL100	S6CS25P	Conv. (kW)	Initial Capital	Operating Cost ($/yr)	Total NPC	COE ($/kWh)	Ren. Frac.
285	6	1350	212	$ 2,299,600	60,339	$ 3,070,934	0.218	1.00

Fig. 20. Optimal hybrid system configuration proposed by HOMER.

Cost Summary | Cash Flow | Electrical | PV | FL100 | Battery | Converter | Emissions | Hourly Data

Production	kWh/yr	%
PV array	559,556	18
Wind turbines	2,504,746	82
Total	3,064,302	100

Consumption	kWh/yr	%
AC primary load	1,103,032	100
Total	1,103,032	100

Fig. 21. Contribution of wind and solar resources in meeting the load.

7 | Conclusion

This study presents a comprehensive modeling and techno-economic assessment of a hybrid wind–solar off-grid system for a remote area in Bandar Lengeh, incorporating detailed site-specific climatic data over a five-year period. The optimal configuration, determined via HOMER, consists of 669 kW of PV arrays, seven 100 kW Fuhrländer wind turbines, 1,775 S6CS25P batteries, and a 209kW power inverter. This configuration achieves a NPC of \$4,825,298 and a Levelized LCOE of \$0.342/kWh. Sensitivity analysis revealed that variations in wind speed and solar irradiance significantly affect the energy contribution of each source, emphasizing the importance of considering climatic variability in the design process. The integration of energy storage mitigates voltage fluctuations and prevents undesired islanding events during transient cloud cover, thereby enhancing system reliability. Moreover, minimizing network impedance emerged as a critical factor for stable operation under high renewable penetration. Overall, the findings demonstrate that properly sized HRES, supported by adequate energy storage, can provide a technically reliable and economically viable solution for supplying electricity to remote or off-grid regions.

Acknowledgments

The author extends sincere appreciation to the specialists and practitioners in renewable energy and microgrid design whose discussions and technical insights contributed to refining the modeling approach. The author also gratefully acknowledges the anonymous reviewers and the editorial team of Intelligence Modeling in Electromechanical Systems for their constructive feedback and careful evaluation, which significantly improved the clarity and quality of this work.

Funding

This research was conducted without financial support from governmental, commercial, or non-profit funding bodies. All simulations and analyses were carried out independently.

Data Availability

The analysis in this study is based on simulation results generated in HOMER software using meteorological and technical parameters described in the article. Processed datasets and simplified versions of the simulation models can be provided by the corresponding author upon reasonable request.

References

[1] Eltamaly, A. M., Alotaibi, M. A., Alolah, A. I., & Ahmed, M. A. (2021). A novel demand response strategy for sizing of hybrid energy system with smart grid concepts. *IEEE access*, *9*, 20277–20294. https://doi.org/10.1109/ACCESS.2021.3052128

[2] Samy, M. M., Mosaad, M. I., El-Naggar, M. F., & Barakat, S. (2021). Reliability support of undependable grid using green energy systems: Economic study. *IEEE access*, *9*, 14528–14539. https://doi.org/10.1109/ACCESS.2020.3048487

[3] Sawle, Y., Jain, S., Babu, S., Nair, A. R., & Khan, B. (2021). Prefeasibility economic and sensitivity assessment of hybrid renewable energy system. *IEEE access*, *9*, 28260–28271. https://doi.org/10.1109/ACCESS.2021.3058517

[4] Shaheen, M. A. M., Hasanien, H. M., & Al-Durra, A. (2021). Solving of Optimal Power Flow Problem Including Renewable Energy Resources Using HEAP Optimization Algorithm. *IEEE access*, *9*, 35846–35863. https://doi.org/10.1109/ACCESS.2021.3059665

[5] Verma, A., & Singh, B. (2019). *An implementation of renewable energy based grid interactive charging station*. 2019 IEEE transportation electrification conference and expo (ITEC) (pp. 1–6). IEEE. https://doi.org/10.1109/ITEC.2019.8790455

[6] Ravada, B. R., Tummuru, N. R., & Ande, B. N. L. (2021). Photovoltaic-wind and hybrid energy storage integrated multi-source converter configuration for DC microgrid applications. *IEEE transactions on sustainable energy*, *12*(1), 83–91. https://doi.org/10.1109/TSTE.2020.2983985

[7] Narayanan, V., Kewat, S., & Singh, B. (2021). Control and implementation of a multifunctional solar PV-BES-DEGS based microgrid. *IEEE transactions on industrial electronics*, *68*(9), 8241–8252. https://doi.org/10.1109/TIE.2020.3013740

[8] Rao, T. E., Sundaram, E., Chenniappan, S., Almakhles, D., Subramaniam, U., & Bhaskar, M. S. (2022). Performance improvement of grid interfaced hybrid system using distributed power flow controller optimization techniques. *IEEE access*, *10*, 12742–12752. https://doi.org/10.1109/ACCESS.2022.3146412

[9] Krishna, K. H., Prudhviraj, I. V. N. S. M., Prabhavathi, J., Kartheek, M., & Gopi, K. S. (2021). Performance investigation of multifunctional hybrid wind-solar PV-BES-DEGS based microgrid system with EAF and SOGI based control. *2021 Innovations in power and advanced computing technologies (i-PACT)* (pp. 1-8). IEEE. https://doi.org/10.1109/i-PACT52855.2021.9696491

[10] Ramkumar, M. S., Swapna, G., Saravanan, A., Hemalatha, N., Dharmaraj, G., Purushotham, S., & Sivaramkrishnan, M. (2021). *Super capacitor based solar and wind grid connected storage system*. 2021 third international conference on inventive research in computing applications (ICIRCA) (pp. 218–225). IEEE. https://doi.org/10.1109/ICIRCA51532.2021.9544604

[11] AlKassem, A., Ahmadi, M. Al, & Draou, A. (2021). *Modeling and simulation analysis of a hybrid pv-wind renewable energy sources for a micro-grid application*. 2021 9th international conference on smart grid (ICSMARTGRID) (pp. 103–106). IEEE. https://doi.org/10.1109/icSmartGrid52357.2021.9551215

[12] Ghosh, S., Barman, J. C., & Batarseh, I. (2021). *Model predictive control of multi-input solar-wind hybrid system in dc community with battery back-up*. 2021 IEEE 12th international symposium on power electronics for distributed generation systems (PEDG) (pp. 1–8). IEEE. https://doi.org/10.1109/PEDG51384.2021.9494234

[13] Ali, H. H., Kassem, A. M., Al-Dhaifallah, M., & Fathy, A. (2020). Multi-verse optimizer for model predictive load frequency control of hybrid multi-interconnected plants comprising renewable energy. *IEEE access*, *8*, 114623–114642. https://doi.org/10.1109/ACCESS.2020.3004299

[14] Rampradesh, T., & Rajan, C. C. A. (2021). *Performance assessment of nmpc based mppt controller and extended kalman filter for a wind/pv hybrid system*. 2021 fourth international conference on electrical, computer and communication technologies (ICECCT) (pp. 1–4). IEEE. https://doi.org/10.1109/ICECCT52121.2021.9616873

[15] Alam, M. J. E., Muttaqi, K. M., & Sutanto, D. (2014). A novel approach for ramp-rate control of solar PV using energy storage to mitigate output fluctuations caused by cloud passing. *IEEE transactions on energy conversion*, *29*(2), 507–518. https://doi.org/10.1109/TEC.2014.2304951

[16] Ari, G. K., & Baghzouz, Y. (2011). *Impact of high pv penetration on voltage regulation in electrical distribution systems*. 2011 international conference on clean electrical power (ICCEP) (pp. 744–748). IEEE. https://doi.org/10.1109/ICCEP.2011.6036386

[17] Bakhiyi, B., Labrèche, F., & Zayed, J. (2014). The photovoltaic industry on the path to a sustainable future-Environmental and occupational health issues. *Environment international*, *73*, 224–234. https://doi.org/10.1016/j.envint.2014.07.023

[18] Das, N., Wongsodihardjo, H., & Islam, S. (2015). Modeling of multi-junction photovoltaic cell using MATLAB/Simulink to improve the conversion efficiency. *Renewable energy*, *74*, 917–924. https://doi.org/10.1016/j.renene.2014.09.017

[19] Aissou, S., Rekioua, D., Mezzai, N., Rekioua, T., & Bacha, S. (2015). Modeling and control of hybrid photovoltaic wind power system with battery storage. *Energy conversion and management*, *89*, 615–625. https://doi.org/10.1016/j.enconman.2014.10.034

[20] Fialho, L., Melício, R., Mendes, V. M. F., Viana, S., Rodrigues, C., & Estanqueiro, A. (2014). A simulation of integrated photovoltaic conversion into electric grid. *Solar energy*, *110*, 578–594. https://doi.org/10.1016/j.solener.2014.09.041

[21] Sun, K., Zhang, L., Xing, Y., & Guerrero, J. M. (2011). A distributed control strategy based on DC bus signaling for modular photovoltaic generation systems with battery energy storage. *IEEE transactions on power electronics*, *26*(10), 3032–3045. https://doi.org/10.1109/TPEL.2011.2127488

[22] Zhang, L., Sun, K., Xing, Y., Feng, L., & Ge, H. (2011). A modular grid-connected photovoltaic generation system based on DC bus. *IEEE transactions on power electronics*, *26*(2), 523–531. https://doi.org/10.1109/TPEL.2010.2064337